Int. J. Electrochem. Sci., 9 **(2014)** 4331 - 4344

International Journal of
ELECTROCHEMICAL
SCIENCE
www.electrochemsci.org

Effect of Segmented Current Collection Contacts Attached to Gas Diffusion Layer in Micro PEM Fuel Cells with Ceramic Flow Field Plates

P. Ramesh[*] *, S.P Duttagupta*

Dept of Electrical Engineering, Indian Institute of Technology Bombay, Maharashtra ,India 400076
[*]E-mail: ramp@ee.iitb.ac.in

Received: 27 March 2014 / *Accepted:* 29 April 2014 / *Published:* 19 May 2014

Proton exchange membrane fuel cells (PEMFCs) are very promising for power stationary applications. One of the key components of fuel cells is the flow field plate through which hydrogen fuel will reach the anode and oxygen reach the cathode. Another function of the flow field plate is the electron collection. Traditionally flow field plates are made of graphite which makes them good for current collection. But graphite is costly and the alternative steel is heavy. Thus with development of MEMS technology it becomes important to have flow field plates made of silicon or ceramics. As silicon and ceramics are not good electrical conductors, electrical contacts have to be attached to the Gas Diffusion Layer (GDL) for taking the power to outside world. This is achieved by attaching contact pads to the GDL area which are not covered by flow plates. A reduction in the power output from the cell is observed with current collection from the GDL. Here we build a three dimensional model for a fuel cell in which current collection is carried out by segmented contacts attached to the GDL and the reasons for drop in performance is studied. Also the current collection contact is segmented in order to increase the power output from the cell

Keywords: PEM Fuel cell; 3-D modeling; segmented contacts; Gas Diffusion layer; Membrane Electrode Assembly.

1. INTRODUCTION

Fuel cells [1] are emerging as the power sources of the future. PEM fuel cell [2] are the most popular type of fuel cells which use hydrogen as the fuel. The necessary improvements for fuel cell operation [3] and performance demands better design and optimization. These issues can be addressed easily if mathematical models [7-9, 10] are available. Traditionally the flow field plates are made of graphite and the current collection is carried out from the flow field plates. But in literature, many

authors [4-6] have reported building micro fuel cells, where the flow field plates are also made of silicon.

United States patent No. US 6,821,666 by Jeffrey D. Morse in 2004 reports a structure fabricated in LTCC wherein a thin film fuel cell can be embedded. It uses micro porous ceramic as a gas diffusion layer to supply fuel to thin film fuel cell. In the work reported here, a PEM fuel cell is used, which uses carbon paper as a gas diffusion layer, hence the package requires no additional GDL. Instead the fuel and air is supplied by serpentine manifolds formed in LTCC layers which are proved to remove the water effectively thereby avoiding the flooding in fuel cell. Lee et al [27] reported a flip flop micro fuel cell with a power density of 40 mW/cm^2 process was very difficult. Yua et al [28] fabricated a miniature fuel cell which consisted of a membrane–electrode-assembly (MEA) between two silicon substrates. The feed holes and channels in the silicon wafers, acting as a fuel distributor, were in which fuel is routed in cross patterns. The fabrication prepared by anisotropic silicon etching from the back and front of the wafer using silicon dioxide as an etching mask. In an attempt to reduce the cell resistance and consequently improving cell performance of the miniature silicon wafer fuel cell, a Cu/Au composite layer was sputtered on the top of silicon wafers as a current collector. The peak power density of the cell was 107.3 mW/cm^2 respectively. Shah et al [29] successfully fabricated hydrogen–air micro proton exchange membrane fuel cells (PEMFC) on silicon and poly dimethyl siloxane (PDMS) base substrates. They registered open circuit voltage in excess of 0.790 V while the peak power of 0.282 mW at 0.375 V was obtained from this fuel cell. Park et al. [30] pyrolyzed carbon fluidic plates with feature sizes less than 1 mm to create a miniature fuel cell. Epoxy is used to seal the fuel cell and water is directly applied to exposed Nafion to hydrate the membrane. The use of miniature carbon fluidic plates will allow for fabrication of 3D (non-planar) proton exchange membrane fuel cells utilizing carbon bipolar plates. The maximum power output is 0.773 mW when tested with methanol as a fuel at 260 mA/cm^2. Here we are trying to make a pem fuel cell with ceramic flow field plates and carry out current collection from the GDL as ceramic is a bad conductor of electricity.

Various researchers have performed simulation studies [12,13] on the effects of flow-channel geometric parameters on cells with varying channel dimensions. Palaniappan etal [26] investigated the effect of mal flow distribution in PEM fuel cells and reported performance loss as a result of non uniform fuel distribution across the reaction sites. Ramesh et al [31,32] studied the effect of channel dimensions on micro PEM fuel cell performance and reported decreasing performance with increasing channel widths. Scholta et al [23] predicted that narrow channels are preferable for high current densities, whereas wider channels are favored at low current densities. Shimpalee et al [20,24] showed that the flow-channel path length and other channel geometric dimensions affect cell performance .They also found that too deep channel depth tend to reduce the local gas pressure, leading to variances in fuel distributions. Wang et al [21] build a numerical model for a PEM fuel cell with serpentine channels and studies the effect of channel dimensions. Kumar et al [18] studied the effect of channel dimensions and shape on pem fuel cell performance .The studies by Feng et al [13] revealed that the performance of a PEMFC with a serpentine flow channel is insensitive to channel depth in certain operation conditions. Investigations by Manso et al [25] on the effects of the aspect ratio (defined as the ratio of channel depth to width) on the performance of miniature cell indicated that cells with a

high aspect ratio yield higher current densities. This result differs from other simulation results, in which channel depth had no significant effects [22,23]. This disagreement may result from the differences in channel scales. Deeper channel depths provide sufficient space for reactant transportation and water removal. However, it also enlarges the channel cross-sectional area and slow down flow velocity, which subsequently affects mass transfer rate and water balance in the membrane electrode assembly Although numerous papers [12,15-17] explore flow channel geometric variables using two dimensional simulation , only a few papers [8,13,14,19] have dealt with three dimensional simulation, especially in miniature scale. It is more challenging to implement a three dimensional fuel cell model and examine the effects of segmented contacts on efficient miniature fuel cells. From these reviews, it can be concluded that the effective rib area has got a significant role in pem fuel cell performance. So while dealing with current collection from the GDL, special care must be given so as not to reduce the effective rib area.

In this paper, we try to implement a 3 D model of a PEM fuel cell with segmented current collection from the GDLThe study was done further without changing the effective rib area. The no. of segmented contacts analysed varies from 3, 5 and 7. With varying the contacts the power output were observed and the reason for performance variation is analysed

2. GOVERNING EQUATIONS FOR THE FUEL CELL MODEL

The gas flow within the channel is assumed to take place by convection and diffusion .The gas flow in the gas channel is modeled with the momentum and continuity equations (Navier-Stokes equations):

$$\frac{\partial(\varepsilon\rho u)}{\partial t} + \nabla.(\varepsilon\rho uu) = -\varepsilon\Delta p + \nabla.(\varepsilon\mu^{eff}\Delta u) + S_u \qquad (1)$$

$$\frac{\partial(\rho\varepsilon)}{\partial t} + \nabla.(\varepsilon\rho u) = 0 \qquad (2)$$

where ε is the porosity ,μ the dynamic viscosity, (Pa.s), ρ the density (Kg/m^3),S_u is the source term (for any external force),p is pressure (Pa),u – gas velocity vector (m/s).

Navier Stokes equations are applied in the gas channel with source term equal to zero while it is added as Darcy law in the GDL and catalyst layer to describe the flow in the porous media (Darcy law) along with the viscous effects that are important at the boundary between flow channel and GDL.

The mass flux in the gas phase is based on the Maxwell-Stefan diffusion and convection equations. It is described by this expression for species j:

$$\nabla.(\rho X_i u) = \nabla.(\rho\sum_{j=1}^{n-1} D_{ij}^{eff}\nabla X_j) + S_i \qquad (3)$$

Where D_{ij}^{eff} is the effective diffusion constant.

Since gas diffusion layers (GDL) and catalyst layers are porous media, the velocity distribution is therefore formulated by Darcy's law and mass conservation equation.

Darcy's Law:

$$u = -\frac{\kappa}{\mu}\nabla P \qquad (4)$$

where κ is the permeability, m^2; and μ the dynamic viscosity, Pa.s;

The continuity of current in a conducting material is described by

$$\nabla . i = 0 \qquad (5)$$

In a PEM fuel cell, the conducting materials are porous electrodes and membrane. The current is therefore split into two parts: the ionic current and the electronic current. Protons travel through the ionic conductor (the membrane) to form an ionic current denoted by i_e, while electrons can only be transferred through the solid matrix of electrodes which results in an electronic current denoted by i_s. The continuity equation of current then becomes:

$$\nabla . i = \nabla . i_s + \nabla . i_e 0 \qquad (6)$$

In the catalyst layer, where a chemical reaction occurs on a three-phase boundary, electrons are either transferred from the solid matrix to electrolyte or vice versa. This two-way transfer of electrons between solid matrix and electrolyte makes the transfer current density, denoted by j, a source term in one phase, and a sink term in the other phase. The potential equations for both solid and electrolyte phases are obtained by applying Ohm's law to Eq. (12).

Electron transport

$$\nabla .(\sigma_s^{eff} \nabla \phi_s) + S_{\phi s} = 0 \qquad (7)$$

Proton transport

$$\nabla .(\sigma_m^{eff} \nabla \phi_m) + S_{\phi e} = 0 \qquad (8)$$

Where ϕ is the phase potential, σ_m^{eff} is the effective electric conductivity or also can be termed as the ionic conductivity in the membrane given by S/m; σ_s^{eff} is the effective electrode conductivity,

S the current source term, A/m^3; the subscript s denotes the property of a solid phase and e denotes that of an electrolyte phase. The source terms in the electron and proton transport equations, i.e., Eq. (13-14), result from the electrochemical reaction occurring in the catalyst layers of anode and cathode sides. The effective conductivity σ_m^{eff} is given by

$$\sigma_m^{eff} = \varphi_m^{1.5} e^{1268\left(\frac{1}{303}-\frac{1}{T}\right)}.(0.5139\lambda - 0.326) \; ; \lambda > 1 \qquad (9)$$

$$\sigma_m^{eff} = \varphi_m^{1.5} e^{1268\left(\frac{1}{303}-\frac{1}{T}\right)}(0.1879) \quad \text{for} \quad \lambda \le 1$$

Where φ_m - Volumetric fraction of ionomer in the catalyst layer, T is absolute temperature in Kelvin,

λ is the water content in the membrane phase which is related to the activity of water vapor in the adjacent pores, given by $a = \chi_{H2O}\frac{P}{P_{sat}}$,P is the gas pressure, P_{sat} is the saturation gas pressure, χ_{H2O} is the gas phase water mass fraction)

Using an experimentally derived relationship by Springer for Nafion 117 membrane

$\lambda=0.043 + 17.81a - 39.85a^2 + 36a^3$ for $0\leq a\leq 1$ (10)

$\lambda=14 + 1.4(a-1)$ for $a>1$

The source terms are

Anode catalyst layer and Cathode catalyst layer

$$S_{\phi s} = -j_a S_{\phi s} = -j_c \qquad (11)$$

$$S_{\phi e} = j_a S_{\phi s} = j_c \qquad (12)$$

Where j_a and j_c are the transfer current density corresponding to the electrochemical reaction at the anode and cathode catalyst layers. The transfer current densities are given by Butler-Volmer equations

$$j_a = Aj_{0,a}^{ref}\left(\frac{C_{H2}}{C_{H2}^{ref}}\right)\left(e^{-\alpha_{c,a}\eta_a F/RT} - e^{\alpha_{a,a}\eta_a F/RT}\right) \qquad (13)$$

$$j_c = Aj_{0,c}^{ref}\left(\frac{C_{O2}}{C_{O2}^{ref}}\right)\left(e^{-\alpha_{c,c}\eta_a F/RT} - e^{\alpha_{a,c}\eta_a F/RT}\right) \qquad (14)$$

A – electrode active surface area in m^2

η – activation overpotential

F – Faraday's constant

R – universal gas constant

T- absolute temperature in Kelvin

j_0 – exchange current density A/m^2

3. EXPERIMENTAL

The Nafion 212 membrane was boiled in 3% H_2O_2 solution for 1 hour. Then membrane was placed in deionized water and boiled for 1 hour. Again membrane was boiled in 0.5 M H_2SO_4 solution and again boiled in deionized water. The membrane is ready for use now. Two pieces of Toray carbon paper were cut in size of 2.2cm x 2.2cm.Amorphous carbon Vulcan XC- 72 of weight was ultrasonicated in isopropanol to which PTFE dispersion was added, which varies from 15 to 30 wt% to make the slurry. This slurry was then brushed on carbon paper pieces and dried at 80^o C to make GDL.The above steps were repeated with platinized carbon from E-Tek. 20% weight of platinum on carbon. Nafion concentration was kept fixed at 30 wt % of catalyst. Platinum loading was 0.2 mg/ cm^2 on anode and 0.4 mg / cm^2 on cathode. Now the two electrodes are ready and placed the membrane in between the two electrodes, which was sandwiched between 2mm thick Teflon sheets and hot pressed the assembly together for 2 min under 50 atm of pressure, at approx 125 degrees.

The MEA is tested in Arbin Instruments fuel cell test station with 100 % humidified oxygen and hydrogen gas. Flow rates were maintained at 0.2 SLPM. The gas was passed for 15 min to completely humidify the membrane after which a constant current was drawn in the intervals of five minutes and voltage is noted. Impedance spectroscopy was performed in galvanostatic mode for current densities upto 1.2 A/cm^2 where anode is used as a reference and counter electrode whereas cathode served as a working electrode.

4. THE MODEL

A 3 dimensional model of a PEM fuel cell is implemented using COMSOL Multiphysics. The present model is established based on the following assumptions:

- Flow is laminar everywhere due to small gas pressure gradient.
- Reactant gases behave as the ideal gas mixture.
- The electrodes and membrane are made of homogeneous materials.
- The temperature distribution across the cell is uniform.
- Water exists only in the gas phase in the fuel cell.
- The polymer electrolyte membrane is impermeable to reactant gases.
- Protons can only transport through the electrolyte, and electrons through the solid phase.
- Three species including oxygen, water and nitrogen are considered on the cathode side while only hydrogen and water are considered on the anode side.
- The fuel cell is operating at the steady state.

Figure 1 shows the structure of the model developed in Comsol Multiphysics. The top part is the anode side while bottom part corresponds to the cathode.

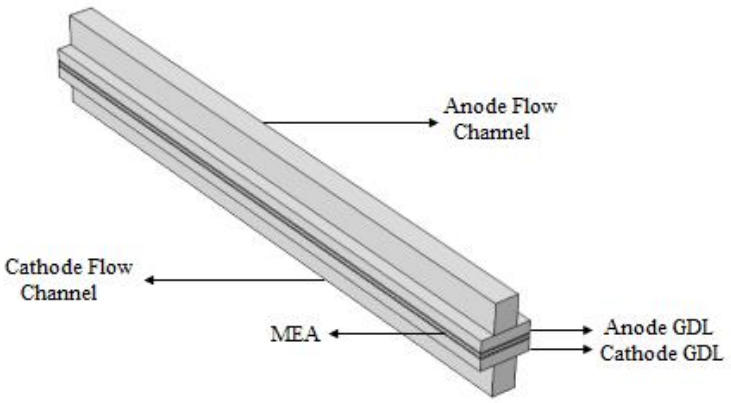

Figure 1. The schematic PEM fuel cell model

The following are the operating conditions of the model.

- Cell Length 0.02m
- Channel height 0.001m
- Channel width 0.7mm
- Rib width 0.9mm
- GDL width 0.3mm
- Contact dimension for 1 contact 200um
- Porous electrode thickness 0.5mm
- Membrane thickness 0.05mm
- GDL Porosity 0.4
- GDL electric conductivity 1000S/m
- Contact electric conductivity 100000S/m
- Inlet H_2 mass fraction (anode) 0.743
- Inlet H_2O mass fraction (cathode) 0.023
- Inlet oxygen mass fraction (cathode) 0.228
- Anode inlet flow velocity 0.2m/s
- Cathode inlet flow velocity 0.5m/s
- Anode viscosity 1.19 E-5 Pa.s
- Cathode viscosity 2.46 E -5 Pa.s
- Permeability (porous electrode) 2.36 E -12 m^2
- Membrane conductivity 10 S/m

Four different ways of connecting contacts to GDL is analyzed in the current study. In the study the effective rib width is kept constant by reducing the contact dimensions with increasing number of contacts. 3-D models for all the four schemes were also developed. TABLE 1 shows the various schemes of current collection.

Table 1. Schemes of current collection

Case No	No.of Contacts	Contact Dimension	Contacts Position
1	1	200 µm	Center
2	3	66.667 µm	Evenly distributed
3	5	40 µm	Evenly distributed
4	7	28.5 µm	Evenly distributed

Figure 1 shows the structure of the model and figure 2 shows the structure of the model with segemented contacts.Case 1 shows the schematic with a single contact having contact dimension of 200 µm and the contacts are placed towards the centre. In case 2, the single contact is segmented in three contacts with dimensions 66.6 µm and the contacts are uniformly placed across the GDL. In case

3, the number of contacts is increased to five and distributed uniformly throughout the GDL. In case 3, the contact dimensions are fixed as 40 µm. In case 4, seven contacts are distributed uniformly across the GDL and the contact dimension is fixed as 28.5 µm. By reducing the contact dimension, the effective rib area is not affected.

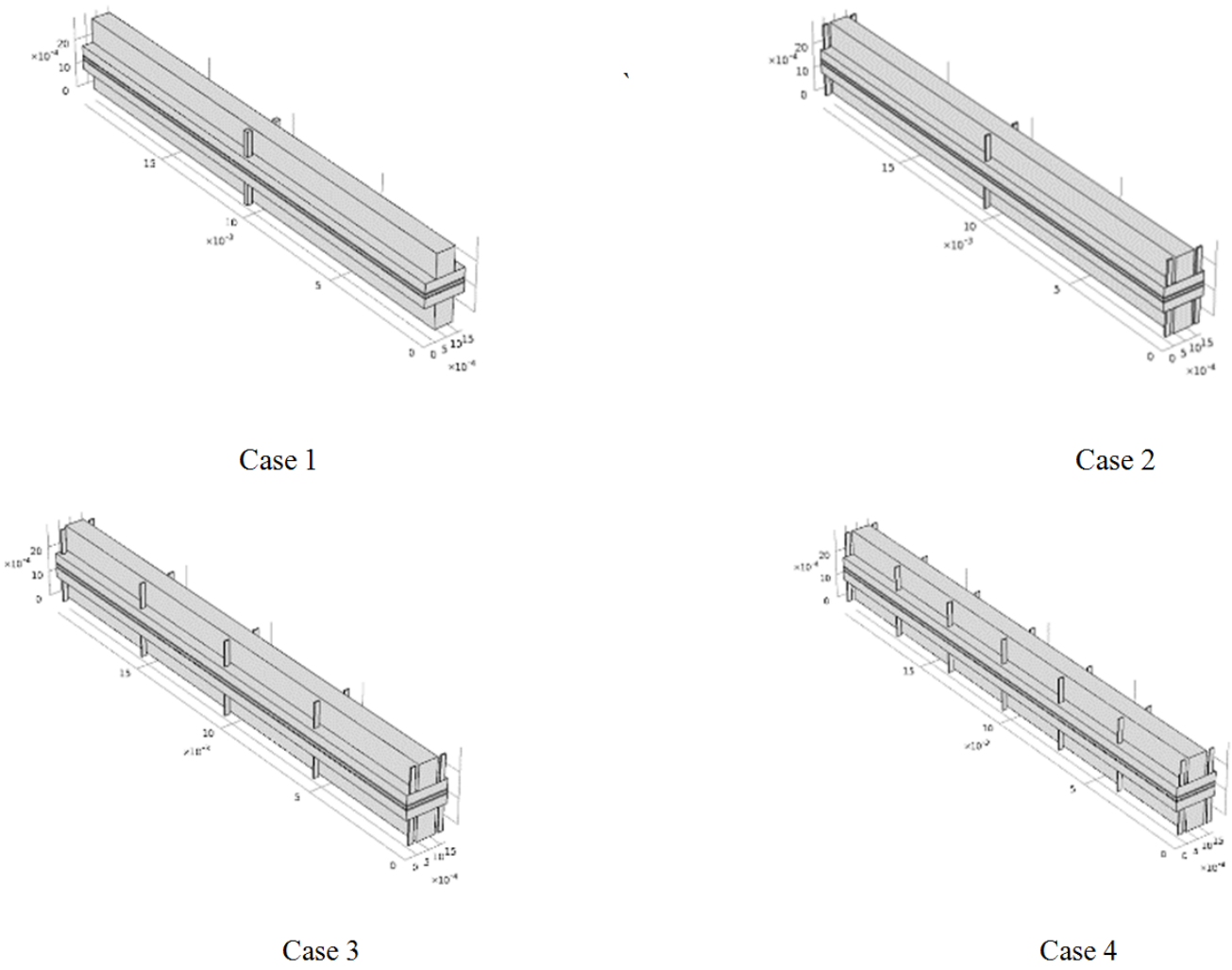

Figure 2. PEMFC models with segmented contacts

5. RESULTS

Figure 3 shows the experimental and modeled polarization plot. Fitting is obtained by varying active surface area of the catalyst per unit volume and cathodic Tafel slope. Membrane conductivity was determined from the high frequency intercept in the Nyquist plot, assuming negligible contact resistance. Its estimated value is 10 S/m over the modeled current density range. Impedance spectroscopy in Fig 4 shows the Nyquist plot for the MEA. Following observations can be made from these plots.

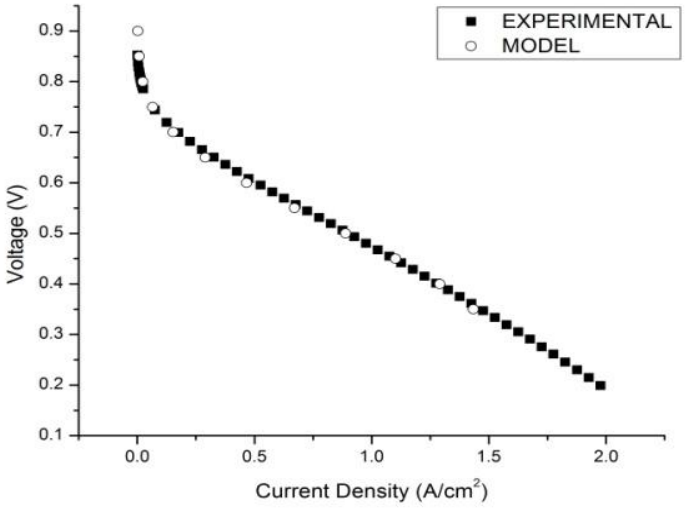

Figure 3. Polarization plot for experimental and modelling results

1. For all current densities HFR is nearly the same which means no change in membrane conductivity. But there is slight increase in HFR above current density of 1 A/cm^2, which may be due to gradient of water across the membrane due to higher production rate of water at the cathode.

2. Mid frequency arc diminishes as current density increases. This is due to decrease in charge transfer resistance which is related to the faster kinetics of oxygen reduction at high current densities. This behavior is observed upto current density of 1.2 A/cm^2, the mid frequency arc starts increasing after this. This may be attributed to oxygen mass transport limitations due to water accumulation on the cathode side.

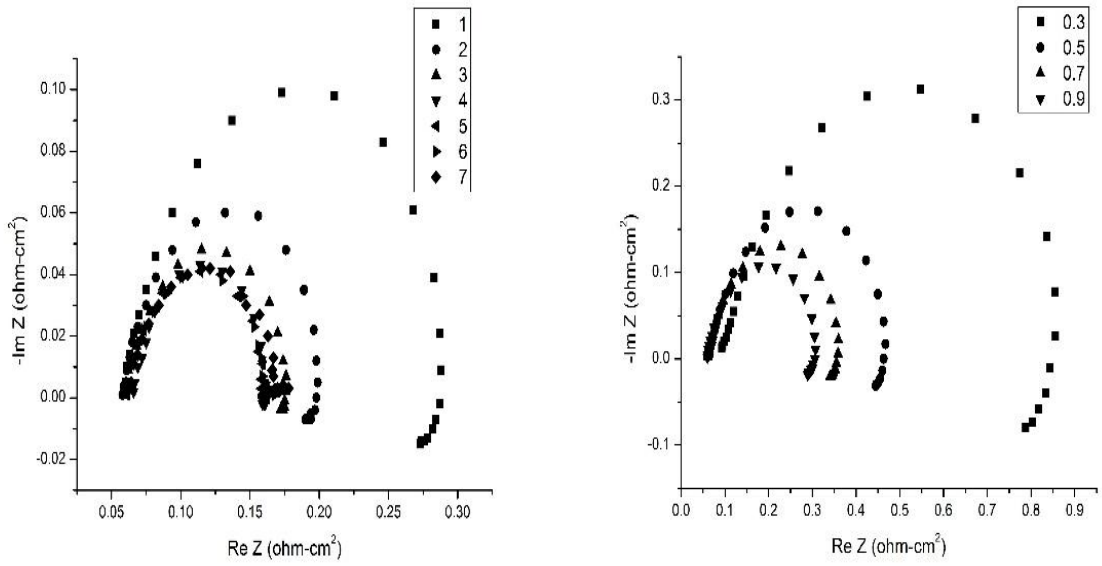

Figure 4. Nyquist plots of the measured values assigned to the markers refers to the total current

The fabricated cell produced a peak power density of 100 mW/cm^2.This is less when compared to the conventional cell with graphite flow field plates and current collection from flow pates. But the performance was better when compared with micro fuel cells reported in the literature[4-6, 29, 30].The reasons for drop in performance while collecting current from GD is not studied in literature. The following sections deal with current collection from GDL and increasing performance by segmenting the current collection contacts

5.1. Effect of segmented Contacts:

The polarization plots for the cases given in Table 1 is given in Figure 5. From figure 5, its observed that the cell in case 4 gave maximum performance.The performance is getting increased with increased number of contacts and reducing contact dimensions.

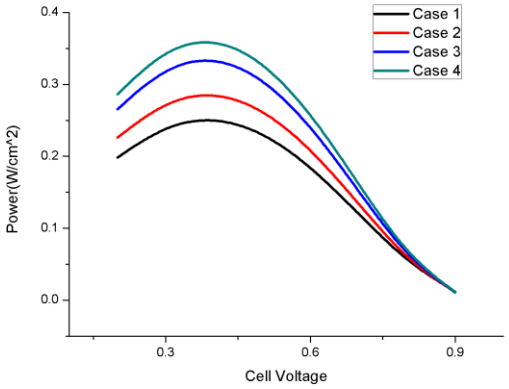

Figure 5. Polarization curves for cases given in Table 1

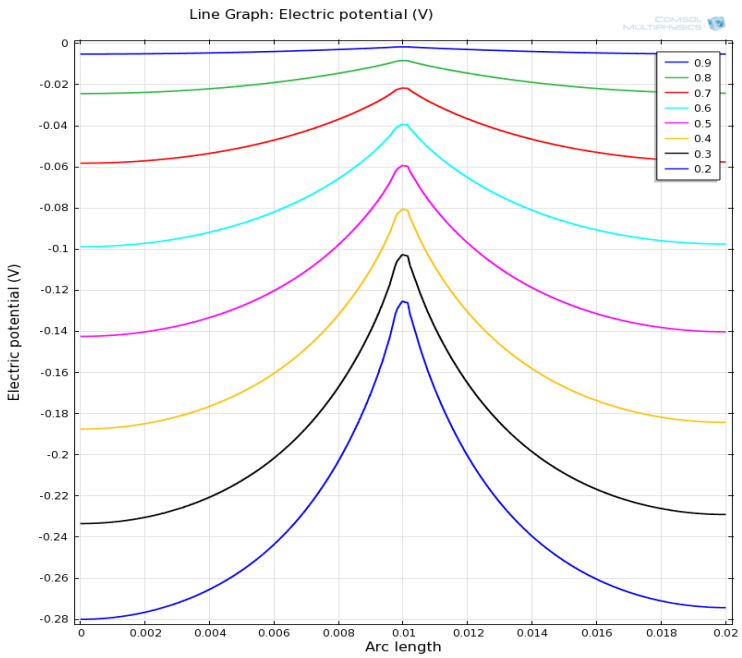

Figure 6. Electrode Potential Variation in case 1

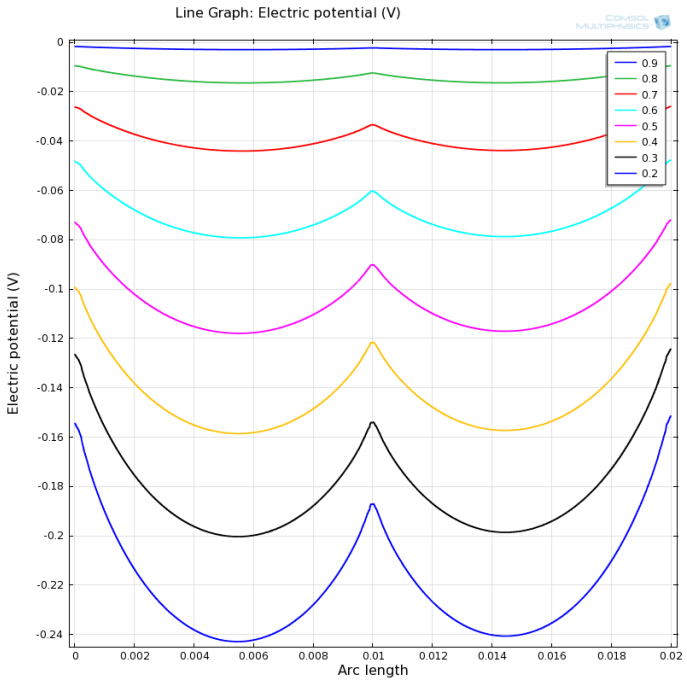

Figure 7. Electric Potential variation with 3 contacts

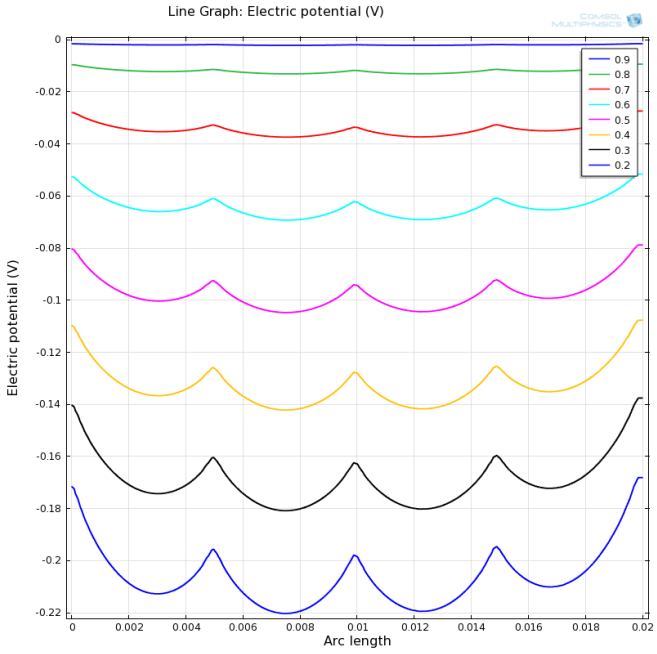

Figure 8. Electric Potential variation with 5 contacts

Figures 6, 7 and 8 shows the electrode potential profiles along the channel in the cathode electrode below the segmented contacts. As can be seen from the graph , the electode potential variation depends on the applied potential and with the number of contacts. It is seen that the drop of electrode potential variation is large for a single contact model than in case of 3 and it is further more than that of a five contact model.

Also the peak values at the points below contacts are also more as the no.of contacts increases. This accounts for the increase in power with segmentation.

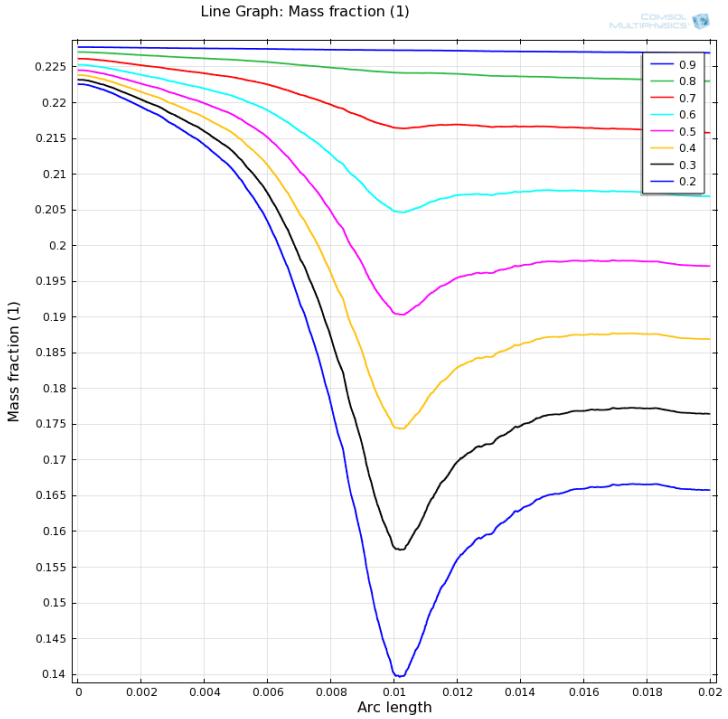

Figure 9. Mass fraction variation with 3 contacts

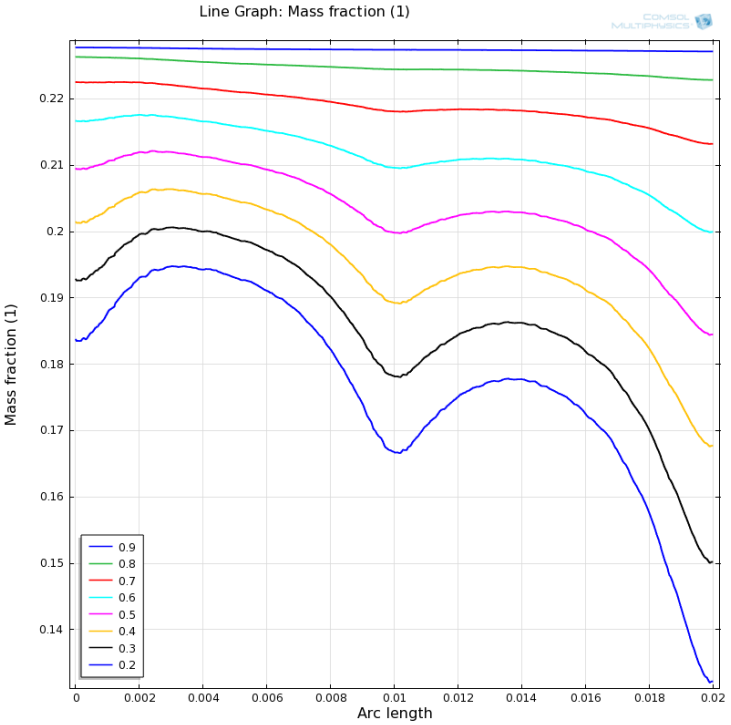

Figure 10. Mass fraction variation with 5 contacts

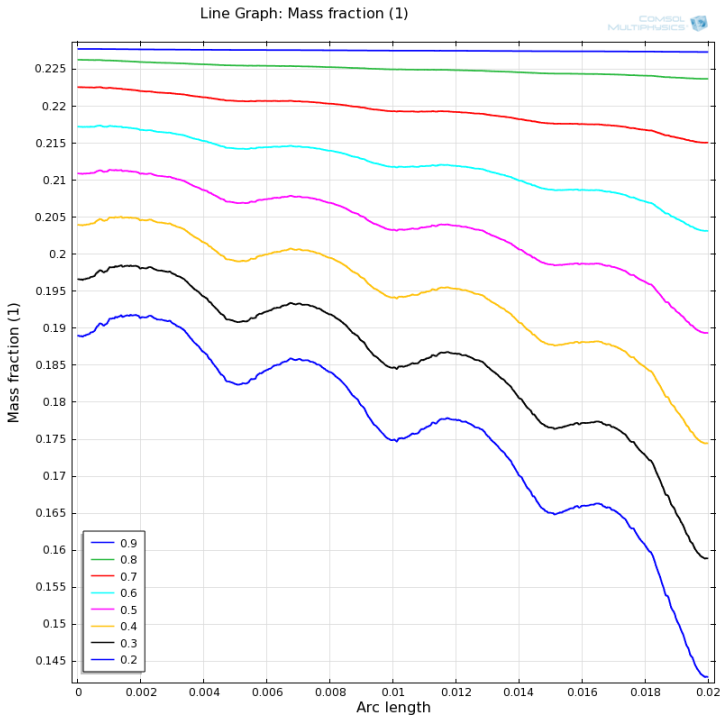

Figure 11. Mass fraction variation with 7 contacts

Figures 9, 10, 11 above shows the oxygen mass fraction variation in GDL below the contacts. Apart from the decrease in the mass fraction towards the outlet, peaks are observed below the gaps in the contacts which indicates the lower current density regions. Also as the no. of contact increases the oxygen mass fraction also increases below the contacts which indicates further higher activity and performance and inturn indicates better power below that regions.

6. CONCLUSION

A 3-dimensional model for PEM fuel cell is validated under the experimentally feasible assumptions. The effect of segmented contacts on the fuel cell performance is studied by considering different cases employing different contact dimensions. Overall performance of the fuel cell is found to be getting increased with segmentation. Segmentation of contacts should be done without affecting the effective rib area. To conclude, the more the segmentation with reduced contact sizing, the more will be the fuel cell performance.

References

1. B Viswanathan , M Aulice Scibioh,Fuel Cells - Principles and applications, Taylor and Francis, New York (2007)
2. Ryan O Hayre, Suk Won Cha, Whitney Collela, Fritz B Prinz ,Fuel Cell Fundamentals, John Wiley and Sons, New York (2005)

3. T.S.Zhao, K.D Kreur .Trung Van Nguyen,Advances in Fuel cells,Elsevier, Great Britain (2007)
4. C.Xie, J.Bostaph,J.Pavio, *Journal of power sources* ,136 (2004) 55
5. Zhen Guoa, Amir Faghri. *Journal of power sources*, 160 (2006) 1183
6. Stefan Wagner, Roger Hahn ,MINATEC (2003)
7. Adrew Rowe, Xianguo Li, *Journal of power sources*,102 (2001) 86
8. S Dutta, S Shimpalee ,J W Van Zee, *Journal of Applied Elecrochemistry* , 30 (2000) 135
9. Sukkee Um, C Y Wang , K S Chen , *Journal of the Electrochemical Society* 147 (2000) 4485
10. Vladimir Gurau, Hongtan Liu, Sadik Kakac, *AIChE Journal*, 44 2004 (2410)
11. A.S.Arico, P.Cretì, V.Baglio, E. Modica, Antonucci, *Journal of Power Sources*, 91(2000) 202.
12. K.S.Cho , H.M.Kim, S.M.Moon, *International Journal of Hydrogen Energy*, 36 (2001) 1613
13. Y.M.Ferng, A.Su, *International Journal of Hydrogen Energy*, 32 (2007) 4466
14. A.Higie , H.Liu, *International Journal of Hydrogen Energy*, 35 (2012) 2144
15. S.S.Hsieh, K.M.Chu,, *Journal of Power Sources*, 173 (2007) 222
16. G.Inoue, Y.Matsukuma, M.Minemoto, *Journal of Power Sources*, 157 (2006) 136
17. D.H.Jeon, S.Greenway, S.Shimpalee, J.W.Van Zee, *International Journal of Hydrogen Energy*, 33 (2008) 1052
18. A.Kumar, R.G.Reddy, *Journal of Power Sources*, 113 (2003) 11
19. J.Lobato, P.Canizares, M.A.Rodrigo, F.J.Pinar, E.Mena, Ubeda, *International Journal of Hydrogen Energy*, 35 (2010) 5510
20. S.Shimpalee, J.W.Van Zee, *International Journal of Hydrogen Energy*, 32 (2007) 842
21. X.D.Wang, W.M.Yan, Y.Y.Duan, F.B.Weng, G.B.Jung, C.Y.Lee, *Energy Conversion and Management*, 51 (2010) 959
22. Y.G.Yoon, W.Y.Lee, G.G.Park, T.H.Yang, C.S.Kim, *Electrochemica Acta*, 50 (2004) 709
23. J.Scholta, G.Escher,W. Zhang, L.Küppers ,L.Jorissen, W.Lehnert, *Journal of Power Sources*, 155 (2006) 66
24. S.Shimpalee, S.Greenway, J.W.Van Zee, *Journal of Power Sources*,160 (2006) 398
25. A.P.Manso, F.F.Marzo, M.G.Mujika, J.Barranco, A.Lorenzo, *International Journal of Hydrogen Energy*, 36 (2011) 6795
26. K.Palaniappan, R.Govindarasu, R.Parthiban , *International Journal of Renewable Energy Research*,2 (2012) 652
27. S. J. Lee, A. Chang-Chien, S. W. Cha, R. O'Hayre, Y. I. Park, Y. Saito, F. B. Prinz, *Journal of Power Sources* 112 (2002) 410.
28. Jingrong Yua, Ping Cheng, Zhiqi Ma , Baolian Yi, *Journal of Power Sources*,10 (2003) 618
29. Keyur Shah, W. C. Shin, R. S. Besser, *Sensors and Actuators B: Chemical* 127 (2004), 157
30. Benjamin Y. Park, Marc J. Madou, *Journal of Power Sources* (2006) 369
31. P. Ramesh, S.S Dimble, S.P Duttagupta, *Comsol Conference,Bangalore* (2011)
32. P. Ramesh, S P Duttagupta , *International Journal of renewable energy research*,3 (2013) 353